STUDYING THE NONSTATIONARY STAGES
OF SCREW ROLLING OF BILLETS
WITH PROFILED ENDS

B. V. Karpov, M. M. Skripalenko, S. P. Galkin,
M. N. Skripalenko, S. V. Samusev, Tran Ba Huy,
and S. A. Pavlov

The rolling of VT-6 alloy billets with profiled ends in a screw rolling mill is studied to determine the geometry of the end sections minimizing the funnel depth after rolling. The rolling experiment conducted is of 2^3 factorial design. The nonstationary stages of the process are simulated using Deform-3D software. The results of the simulation are used to find the shape and dimensions of the end sections of the billet that minimize the funnel depth.

Keywords: *three-high screw rolling, screw rolling minimill, nonstationary stage, funnel, end, profiling, computer simulation, full factorial design.*

One of the effective methods of producing a round billet is screw rolling. Radial-shear rolling (RSR) is a special case of screw rolling at high feed angles (15–18° and more) [1]. RSR provides severe and deep plastic deformation, thus much improving the properties of various, including difficult-to-form and concast, metals and alloys.

Minimills designed by the National University of Science and Technology (MISiS) [2, 3] are widely used for experimental purposes. The RSR process is usually simulated and analyzed using finite-element software. The effect of RSR on the structural formation of a magnesium-alloy billet was studied in [4–6] by simulating the process using Forge 2011[®] software [7]. Another well-known FEM-software, QForm [8], was used in [9] to study the effect of RSR on the formation of gradient structure in copper billets. The structural evolution and ageing of VT-22 alloy after RSR was studied in [10]. LS-DYNA software was used in [11] to analyze the formation of the globular structure of VT-6 alloy billets during RSR. In the literature cited above, the stationary (steady-state) stage of rolling was addressed.

The RSR process includes three stages: main (stationary) stage when there are external undeformed regions at the entry to and at the exit from the deformation zone and two nonstationary stages of deformation of the front and back end sections. A specific feature of the stationary stage is the leveling effect of the external zones on the process in the deformation zone: the peripheral portions of the workpiece are slowed down and its core portion is accelerated [12, 13]. In the process, the elongation ratio remains constant across the billet cross-section and plane sections remain plane (Bernoulli hypothesis). During the deformation of one of the end sections, the deformation zone is filled up (or emptied) in the absence of the leveling effect of one of the external zones. The peripheral portions, which are not restrained by the external zone, lead the core portion. The elongation ratio is no longer constant over the cross-section–the peripheral portions are elongated more than the core. The end faces of the workpiece are subject to intensive warping, resulting in funnel-shaped depressions (funnels).

The formation of a funnel during two-high screw rolling was simulated using various software [14, 15]. Deform-3D was used in [16] to study the formation of a funnel in the back end of steel workpieces with differently shaped ends during RSR. End sections with funnels should be cut off, which inevitably increases the process losses and reduces the yield. It is hardly

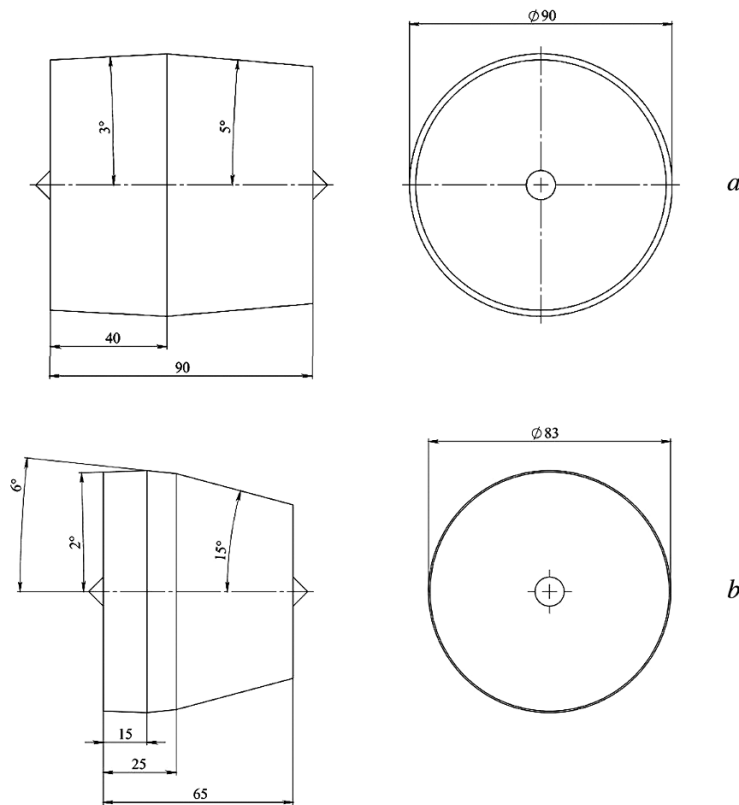Fig. 1. Billets with a diameter of 32 mm and a half end cone angle of 50°.

Fig. 2. Roll design of minimills 14-40 (*a*) and 10-30 (*b*).

possible to prevent the formation of a funnel during rolling of workpieces with flat ends. In this connection, minimizing the funnel depth and, hence, the end crop is an important task. One of the methods to resolve this task is to profile the end face [16].

Our goal here is to shape the end faces of billets so as to prevent the formation of a funnel, considering the diameters of the billet and product.

To *experimentally study* the nonstationary stages of RSR, we used VT-6 titanium alloy billets with conical ends (Fig. 1).

They were rolled on two RSR minimills 14-40 and 10-30 that have work stands of different layouts. The stand of the mill 14-40 has a conventional layout with a feed angle of 20° and a toe angle of 7°. The required pass diameter in the mill is set by radially moving the rolls, at a right angle to the rolling axis [2]. In the stand of the mill 10-30, the angle between the roll axis and the rolling axis is 20° and the rolls are 30 mm offset. The pass is set by moving the rolls axially, i.e., at an angle of 20° to the rolling axis [3]. Both mills exert almost identical forces on the workpiece and implement a trajectory-controlled RSR [12].

TABLE 1. Pass Schedules and Values of the Design Factors

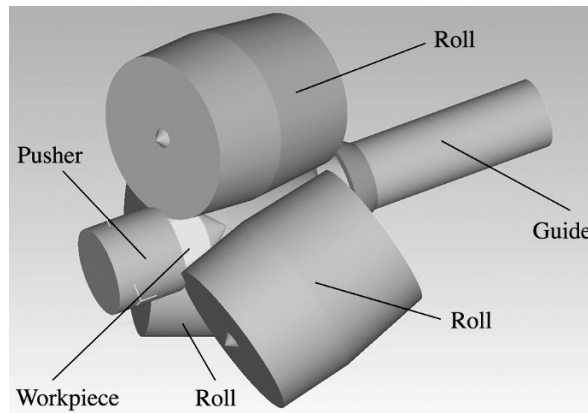| Experiment (schedule) number	Initial billet diameter, mm	Final workpiece diameter, mm	Half end cone angle, deg	Pass schedule
1	45	24	50	∅45→ ∅35→ ∅24
2	32			∅32→ ∅24
3	45	18		∅45→ ∅35→ ∅24→ ∅18
4	32			∅32→ ∅24→ ∅18
5	45	24	20	∅45→ ∅35→ ∅24
6	32			∅32→ ∅24
7	45	18		∅45→ ∅35→ ∅24→ ∅18
8	32			∅32→ ∅24→ ∅18

Fig. 3. Deform-3D model for simulation of the rolling process in the first pass of schedule No. 4 (Table 1).

The roll design is shown in Fig. 2.

The billets were heated to 1050°C and rolled at a roll speed of 90 rpm on the minimill 14-40 and 180 rpm on the minimill 10-30.

The experiments were of 2^3 or 2^k full factorial design [17]. The three factors were half end cone angle, initial billet diameter, final workpiece diameter, each having two values. The design matrix is given by Table 1. Eight tests were run, each replicated three times (three parallel tests) [18].

The billets were rolled from a diameter of 24 mm to 18 mm for the last passes of schedules Nos. 3, 4, 7, and 8 (Table 1) in the minimill 10-30 and the other passes in the minimill 14-40.

Test passes were simulated with Deform-3D [19]. Based on the settings of the minimills 10-30 and 14-40, models of rolls, workpieces, pushers, and guides were generated in SolidWorks [20]. Then the models were exported as stl-files to Deform-3D (Fig. 3). The Deform-3D simulation ignored the heat exchange between the workpiece and the rolls, between the workpiece and the pusher, and between the workpiece and the guides. The heat-transfer coefficient between the metal and the environment was set at 200 W/(m²·K), as recommended in [21]. The coefficient of friction was set at unity for the workpiece–roll pair and at 0.3 for the workpiece–pusher and workpiece–guide pairs, as recommended in [22]. The rolls, pusher, and guides were modeled by rigid bodies.

After test rolling on the RSR minimills and Deform-3D simulation, the funnel depth was measured for each of the

TABLE 2. Funnel Depth after Test Rolling and Deform-3D Simulation

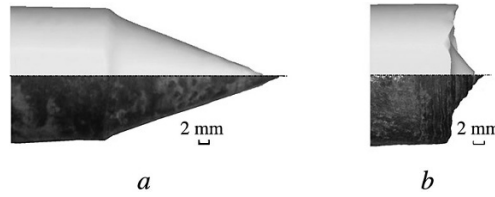| Method	Funnel depth per schedule, mm							
	1	2	3	4	5	6	7	8
Front end								
Test rolling	6	–8	9.5	–4.5	–29	–30.75	–22	–23.5
Deform-3D simulation	3.9	–4.9	8.7	–4.1	–28.3	–27.1	–18.8	–20
Back end								
Test rolling	–5	–8	5	–3.5	–28	–29	–19.5	–23
Deform-3D simulation	–4	–5	2	–1.3	–27.8	–27.8	–17	–20.5

a   *b*

Fig. 4. Comparison of the results of test rolling and Deform-3D simulation: *a*) front end of a $\varnothing$24 mm bar, schedule No. 6 (Table 1); *b*) front end of a $\varnothing$24 mm bar, schedule No. 2 (Table 1); the upper half represents the simulation, and the lower half, the test.

schedules. The simulation and test results are compared in Table 2 and Fig. 4. If the funnel depth is positive (Table 2), then the end defect is a depression; if the funnel depth is negative, then the end defect is a conical projection.

Since the experiment was of 2^3 full factorial design, the regression equations were set up based on the test data [23] to calculate the funnel depth using the values of the end cone angle and the initial and final billet diameters. The statistical analysis has established that the funnels in the front end of $\varnothing$18–30 mm workpieces are 1–3 mm deeper than in the back end. In this connection, the regression equations for the front and back ends differ:

$$y_f = 8.59 - 0.51D - 1.59d - 0.75\alpha_f + 0.032D\alpha_f + 0.02d\alpha_f; \tag{1}$$

$$y_b = -55.29 + 1.05D + 0.74d + 0.38\alpha_b - 0.05Dd + 0.009D\alpha_b, \tag{2}$$

where y_f and y_b are the funnel depths in the front and back ends, respectively, mm; D and d are the initial and final billet diameters, mm; α_f and α_b are the half cone angles in the front and back ends, respectively, deg.

The measured funnel depths and those calculated by Eqs. (1) and (2) are compared in Table 3. It can be seen that the funnel depths in the front and back ends are different. Equating the funnel depths in the front and back ends to zero in the regression equations, we find the half cone angles (α_f and α_b) at which there are no funnels:

$$\alpha_f = \frac{-8.59 + 0.51D + 1.59d}{-0.75 + 0.032D + 0.02d}, \tag{3}$$

$$\alpha_b = \frac{55.29 - 1.05D - 0.74d + 0.05Dd}{0.38 + 0.009D}. \tag{4}$$

To validate the results, we calculated the parameters of the cones for VT-6 alloy billets with an initial diameter of 28 mm and a final diameter of 18 mm. The cone angles on the front and back ends must be 136 and 120°. The workpieces

TABLE 3. Convergence of the Calculated Funnel Depth in the Front and Back Ends Based on Regression Equations

Calculated value, mm	Measured value, mm	Convergence, %
Front end		
5.98	6	0.33
−8.19	−8	2.37
9.52	9.5	0.21
−4.65	−4.5	3.33
−29.12	−29	0.41
−30.81	−30.75	0.20
−21.98	−22	0.09
−23.67	−23.5	0.72
Back end		
−5.03	−5	0.60
−8.93	−8	11.63
4.03	5	19.40
−3.77	−3.5	7.71
−28.58	−28	2.07
−28.97	−29	0.10
−19.52	−19.5	0.10
−23.81	−23	3.52

TABLE 4. Results of Rolling to Minimum and Zero Funnels and Deform-3D Simulation

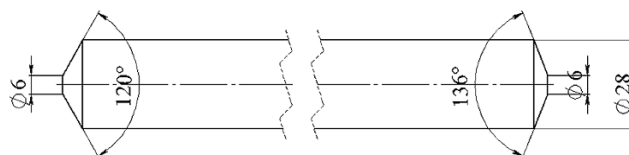| Method	Funnel depth, mm	
	front end	back end
Rolling to minimum funnel		
Test rolling	3.5	−1.3
Deform-3D simulation	6	−1
Rolling to zero funnel		
Test rolling	4.7	−0.6
Deform-3D simulation	6.8	−0.4

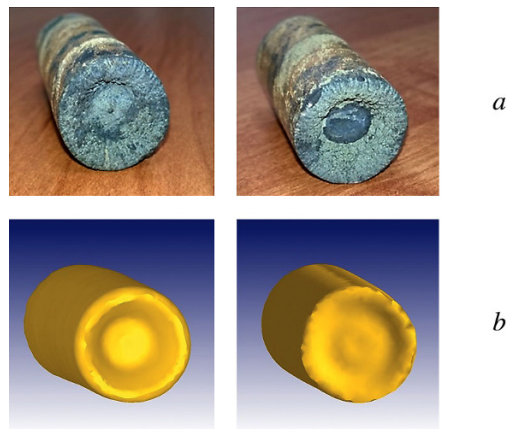Fig. 5. Workpiece with truncated cones on the ends for zero-funnel rolling.

Fig. 6. Workpieces with truncated cones on the front (left) and back (right) ends after rolling from ⌀28 to ⌀18 mm (*a*) and simulation (*b*).

Fig. 7. Ends of workpieces with cone angles of 40° (*a*) and 100° (*b*) after rolling.
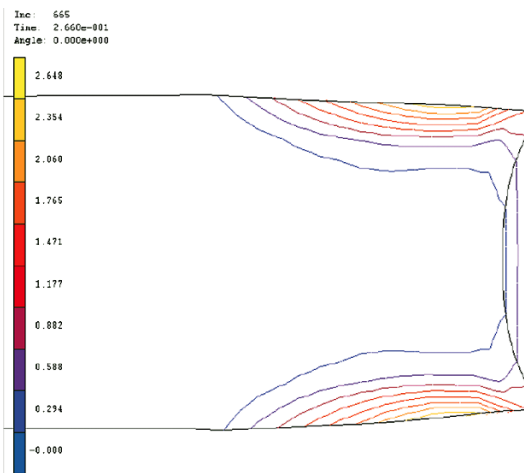

Fig. 8. Distribution of equivalent plastic strain in the near-end zones of the workpiece in simulated three-high screw rolling [25].

were rolled on the mill 14-40 with the same settings as in the 2^3 full factorial experiments. Rolling to zero funnel depth was also simulated in Deform-3D (Table 4).

We failed to obtain a flat end. In this connection, billets of the same initial diameter but with truncated cones on the ends (Fig. 5) were rolled to the same final diameter and simulated in Deform-3D. The results of rolling and simulation are in Table 4 and Fig. 6.

It follows from Table 2 that the Deform-3D simulation results are in better agreement with the experimental data for the workpieces with a cone angle of 40° (schedules Nos. 5–8 in Table 1) than for the workpieces with a cone angle of 100° (schedules Nos. 1–4). The difference between the simulation results and the test rolling data for schedules Nos. 5–8 does not exceed 15%; the difference for schedules Nos. 1–4 is much greater. The cause of the difference in both cases is the different deformation behavior in the near-end zones due to the different end cone angles. The shape of the ends of the workpieces with a cone angle of 40° (Fig. 7*a*) indicates that the deformation behavior in the near-end zone was stable, unlike the workpieces with an end cone angle of 100° whose edges were ragged and irregular (Fig. 7*b*). The Deform-3D simulation is based on the Lagrangian incremental formulation. It can be seen from the results that this method quite accurately describes stable deformation in the near-end zone. If, however, metal flow is unstable, the error of the method is significant. In this connection, other methods should be used to describe the unstable deformation of the billet during screw rolling.

Despite the quantitative disagreement between the simulation results and the test data, they agree qualitatively: in all cases, the simulation properly predicted the formation of either a conical projection or a depression after rolling.

The distribution of temperature over the workpiece has a strong effect on its deformation during RSR. We did not measure the temperature of the workpieces during test rolling. It should be noted that the possible difference between the funnel depths in the ends is due to the difference between the temperatures of the front and back ends. In this connection, it is necessary to measure the temperature during rolling, which will provide additional data for analyzing the causes of the difference between the funnel depths in the ends and creating more accurate models by varying the settings.

In analyzing the results of rolling to minimum funnel, it should be noted that the use of the cone dimensions calculated by the regression equations made it possible to reduce the conical projection in the back end to 1 mm and the funnel in the front end to 3 mm (Table 4 and Fig. 6). The reduction and the end cone angle are likely to have a predominant effect on the formation of the funnel in the back end, according to the factors varied in the full factorial experiment. To produce a funnel of zero or nearly zero depth in the front end, it is necessary to take into account additional factors.

Figure 6 shows a funnel of almost zero depth in the back end whose profile (truncated cone) is qualitatively similar to the distribution of the equivalent plastic strain in the near-end zone of the workpiece during three-high screw rolling predicted with MSC.SuperForm [24] in [25] (Fig. 8). According to [26], the shape of a funnel formed during three-high screw rolling is very similar to a truncated cone.

Conclusions

1. Significant factors contributing to the shaping of the back end of a workpiece during SRS are the reduction and end cone angle. The effect of these factors on the shaping of the front end is significant, yet insufficient. Therefore, to produce a flat front end, additional studies are needed to identify factors affecting the deformation behavior in the near-end zone of the billet.

2. Computer simulation used in studying the formation of a funnel during SRS is effective for predicting qualitative deformation behavior. An accurate quantitative analysis is possible with a method or solver carefully chosen depending on how stable the deformation process in the workpiece is.

3. The truncated conical shape of the front end, which made it possible to produce an almost flat end, is very similar to the shape of the isolines of equivalent plastic strain that characterizes the strain state of the front end of the workpiece during simulated screw rolling and to the shape of the funnel in the ends of the workpiece after three-high screw rolling. These similarities suggest that a truncated cone is the optimal shape of the billet ends for producing flat ends in SRS.

REFERENCES

1. I. N. Potapov and P. I. Polukhin, *Screw Rolling Technology*, Metallurgiya, Moscow (1990).
2. A. V. Goncharuk, B. A. Romantsev, V. K. Mikhailov, et al., Patent 2179900 RF, IPC V21V19/00, "A method and equipment for screw rolling," subm. 04.28.2001, publ. 03.04.2006.

3. S. Galkin, "Radial shear rolling as an optimal technology for lean production," *Steel in Transl.*, **44**, No. 1, 61–64 (2014).

4. M. Diez, H.-E. Kim, V. Serebryany, et al., "Improving the mechanical properties of pure magnesium by three-roll planetary milling," *Mater. Sci. Eng. A*, **612**, 287–292 (2014).

5. A. Stefanik, P. Szota, S. Mroz, et al., "Properties of the az31 magnesium alloy round bars obtained in different rolling processes," *Arch. Metallurgy Mater.*, **60**, No. 4, 3001–3005 (2015).

6. S. Mroz, P. Szota, and A. Stefanik, "The theoretical and experimental analysis of the possibility of employing the groove rolling process for the manufacture of Mg/Al bimetallic bars," *Metallurgy*, **55**, No. 4, 628–630 (2016).

7. Transvalor (2017), www.transvalor.com, acc. 04.20.2017.

8. QForm, www.qform3d.ru, acc. 09.20.2016.

9. Wang Ya Li, A. Molotnikov, M. Diez, et al., "Gradient structure produced by three roll planetary milling: Numerical simulation and microstructural observations," *Mater. Sci. Eng. A, Struct. Mater., Prop., Microstr. Proc.*, **639**, 165–172 (2015).

10. E. V. Naydenkin, I. V. Ratochka, I. P. Mishin, and O. N. Lykova, "Evolution of the structural-phase state of a VT22 titanium alloy during helical rolling and subsequent aging," *Russ. Phys. J.*, **58**, No. 8, 1068–1073 (2015).

11. N. V. Lopatin, G. A. Salishchev, and S. P. Galkin, "Mathematical modeling of radial-shear rolling of the VT6 titanium alloy under conditions of formation of a globular structure," *Russ. J. Non-Ferr. Met.*, **52**, No. 5, 442–447 (2011).

12. S. P. Galkin, Patent 2293619 RF, IPC V21V19/00, "A method of screw rolling," subm. 04.04.2006, publ. 02.20.2007.

13. S. P. Galkin, "Regulating radial-shear and screw rolling on the basis of the metal trajectory," *Steel in Transl.*, **34**, No. 7, 57–60 (2004).

14. S. Fanini, *Modelling of the Mannesmann Effect in Tube Piercing: PhD Thesis* (2008).

15. S. Chiluveru, *Computational Modeling of Crack Initiation in Cross Roll Piercing*, Massachusetts Institute of Technology (2007), pp. 1–89.

16. A. A. Bogatov, D. A. Pavlov, D. V. Ovchinnikov, et al., "FEM simulation and optimization of the new reduction method for continuously cast billet," *Chern. Metally*, No. 11, 26–30 (2013).

17. J. Antony, *Design of Experiments for Engineers and Scientists*, Elsevier (2003).

18. V. A. Voznesenskii, *Statistical Experimental Design Methods in Feasibility Studies*, Finansy i Statistika, Moscow (1981).

19. Scientific Forming Technologies Corporation, www.deform.com, acc. 09.20.2016.

20. SolidWorks, www.solidworks.com, acc. 09.20.2016.

21. Z. Pater and J. Kazanecki, "Complex numerical analysis of the tube forming process using Diescher mill," *Arch. Metallurgy Mater.*, **58**, No. 3, 717–724 (2013).

22. Z. Pater, J. Kazanecki, and J. Bartnicki, "Three dimensional thermo-mechanical simulation of the tube forming process in Diescher's mill (11th Int. Conf. on Metal Forming (Birmingham, England, Sep. 11–13, 2006))," *J. Mater. Proc. Technol.*, **177**, No. 1–3, 167–170 (2006).

23. A. S. Shvedov, *Probability Theory and Mathematical Statistics*, ID GU VShE, Moscow (2005).

24. Simulation of Manufacturing Processes, www.simufact.com/, acc. 09.20.2016.

25. S. Z. Li, W. H. Meng, L. W. Hu, and B. Ding, "Research on the tendency of inner crack during 3-roll skew rolling process of round billets," *Adv. Mater. Res.*, **145**, 238–242 (2011).

26. P. K. Teterin, *Screw Rolling Theory*, Metallurgiya, Moscow (1971).